Available online at www.sciencedirect.com
SCIENCE DIRECT
Journal of Catalysis 232 (2005) 432–443
JOURNAL OF CATALYSIS
www.elsevier.com/locate/jcat

Noble-metal-catalysed aqueous alcohol oxidation: reaction start-up and catalyst deactivation and reactivation

V.R. Gangwal, J. van der Schaaf, B.F.M. Kuster, J.C. Schouten *

Department of Chemical Engineering and Chemistry, Laboratory of Chemical Reactor Engineering, Eindhoven University of Technology, P.O. Box 513, 5600 MB Eindhoven, The Netherlands

Received 10 January 2005; revised 29 March 2005; accepted 31 March 2005

Available online 10 May 2005

Abstract

The influence of the reaction start-up procedure on the oxidation of a polyol, methyl α-D-glucopyranoside, was investigated. Results were obtained from semi-batch experiments with Pt catalysts and molecular oxygen as oxidant. Three types of reaction start-up procedures were applied with respect to the pretreatment of the catalyst slurry: reductive, oxidative, and inert. The experimental results are described by a recently developed dynamic electrochemical kinetic model. The reductive start-up results in the highest initial catalyst activity, compared with the other start-up procedures. It was found that the catalyst needs pretreatment before the reaction is started, as inert start-up resulted in no catalytic activity at all. The formation of inactive platinum oxides (i.e., overoxidation) is the main cause of catalyst deactivation under oxygen-rich conditions, for a weak reducing compound, and is independent of the start-up procedure. It also appeared that the rate of overoxidation is lower in the absence of reaction, which could be modelled with the assumption that overoxidation needs free sites to take place. The mechanism of catalyst deactivation has been verified through intermediate catalyst reactivation. The model adequately describes this reactivation step.

Keywords: Reaction start-up; Catalyst deactivation; Overoxidation; Reactivation; Alcohol oxidation; Electrochemical model

1. Introduction

There is an increasing trend, for heterogeneously catalysed liquid-phase oxidation, toward replacement of stoichiometric quantities of inorganic oxidants [1]. The stoichiometric oxidation process suffers from a low atom efficiency and high toxic waste production [2]. Noble-metal-catalysed oxidations with molecular oxygen are an attractive alternative, as the oxidant is converted to water and the oxidations are in general more selective [3–5]. It is generally accepted that alcohol oxidation on noble-metal catalysts takes place via a dehydrogenation mechanism followed by the oxidation of the adsorbed hydrogen atoms by dissociatively adsorbed oxygen [6–9].

The major obstacle for the large-scale operation of this process is the limited lifetime of the catalyst [10]. The nature of catalyst deactivation is largely influenced by the amount of oxygen present at the catalytic surface. In the oxygen mass transport limited regime, the catalyst surface is reduced, that is, it shows a low electrochemical potential (0.2–0.7 V vs reversible hydrogen electrode, RHE). The rate of alcohol dehydrogenation is low, and the catalyst may deactivate by adsorption of carbonaceous deposits and CO [11–15]. This phenomenon is more pronounced when the catalyst is prereduced by the organic reactant [16–18]. With an increase in the oxygen mass transfer rate, the rate of dehydrogenation increases with increasing electrochemical catalyst potential, and an optimum alcohol dehydrogenation rate can be obtained [14]. However, it is rather difficult to maintain an optimum dehydrogenation rate because the rate of oxygen supply easily exceeds the rate of oxygen consumption, because of the low reactivity of the alcohol compound.

* Corresponding author. Fax: +31 40 2446653.
E-mail address: j.c.schouten@tue.nl (J.C. Schouten).

0021-9517/$ – see front matter
doi:10.1016/j.jcat.2005.03.026

In the intrinsic kinetic regime, the catalyst surface is successively oxidised, leading to the formation of inactive surface oxides, that is, it shows high catalyst potential (∼ 1 V vs RHE). The rate of alcohol dehydrogenation is low, and the catalyst deactivates because of overoxidation [13,19–24]. Depending on the type of reaction and the conditions, other catalyst deactivation mechanisms may exist, such as aldol condensation (polymerisation or coking) [11], metal crystallite growth (Ostwald ripening) [18,21], and metal dissolution (leaching) [17,18,21,22].

The open-circuit catalyst potential measured during the reaction is a direct indication of the oxidation state of the catalyst surface [11,25]. The catalyst potential is mainly influenced by the relative amounts of adsorbed species, such as hydrogen species, oxygen-containing species, and organic species. Mallat and Baiker [26] even suggested that the catalyst potential is a key to controlling alcohol oxidation, and catalyst deactivation can be avoided by proper monitoring of the catalyst potential. Recently, Gangwal et al. [27] successfully demonstrated the ability of a developed electrochemical kinetic model, which uses the relation between the surface coverage and the catalyst potential, to describe the dynamic behaviour of alcohol oxidation. On-line open-circuit catalyst potential measurements showed that catalyst deactivation is accompanied by an increase in the catalyst potential [13,18,21,22,26,27]. However, there is no agreement on the interpretation of the increase in the catalyst potential. It has been attributed to an increase in the oxygen coverage, leading to catalyst deactivation due to overoxidation, and to site coverage by carbonaceous deposits and CO.

Dirkx and van der Baan [28,29] have clearly demonstrated the importance of the start-up procedure for the catalyst activity. It was found that for gluconic acid (weak reducing agent) oxidation on Pt catalyst in a semi-batch reactor, starting with a reduced catalyst resulted in a 14 times higher activity than starting with an oxidised catalyst. However, for glucose (strong reducing agent) oxidation on Pt catalyst, the catalyst activity difference between the two procedures amounted to a factor of only 1.4. Furthermore, Dijkgraaf et al. [20,30] have presented an elementary model for a catalyst deactivation and regeneration process, used for the Pt-catalysed oxidation of sodium-D-gluconate (weak reducing agent). Jelemensky et al. [31] found that, depending on the start-up procedure, multiple steady states can exist during ethanol oxidation in a continuous stirred-tank reactor (CSTR). A low steady-state activity was established with an oxidative start-up, and a high steady-state activity with a reductive start-up. This behaviour was described by a consideration of the transformation of surface oxygen species into subsurface oxygen [32,33].

It is clear that the reaction start-up procedure has a significant influence on the catalytic activity, and interpretation of the measured catalyst potential is important to an understanding of the cause of catalyst deactivation. The goal of this study is to provide detailed quantitative analysis of the effect of reaction start-up and catalyst deactivation during alcohol oxidation under oxygen-rich conditions. Results are obtained with a three-phase stirred slurry semi-batch reactor and Pt-catalysed oxidation of methyl α-D-glucopyranoside, a weakly reducing compound, as a test reaction. Experiments are performed at a constant pH of 8 and a sufficiently high oxygen partial pressure of 40 kPa. A detailed semi-batch reactor model is used to describe and validate the observed catalytic reaction rates. Long-term catalyst deactivation by coking, attrition, crystalline growth, and leaching is not subject of this study. These types of catalyst deactivation are negligible under the chosen experimental conditions. Since the reactor was operated batchwise (i.e., the reactant alcohol concentration was continuously decreasing with time), multiple steady-state behaviour could not be identified and is not part of this study.

2. Modelling

2.1. Kinetic model

In this work the recently developed dynamic electrochemical kinetic model is used [27], which uses the electrochemical potential of the catalyst to describe the experimentally observed data in a heterogeneous catalytic system. The reaction mechanism is presented in Table 1 with the reaction rate equations. The details of the reaction mechanism and the model construction are described elsewhere [27]. The model assumes that catalyst deactivation occurs through strong chemisorption of oxygen, leading to the formation of inactive platinum oxide. The formation of the oxide is represented through steps (VIII) and (IX), Table 1, where $*_s$ denotes oxide formation sites. Throughout the paper this process is referred to as overoxidation. The surface-specific alcohol dehydrogenation rate R_3 (step (III), Table 1) increases with increasing free site fraction, $\Theta*$, and consequently decreases with increasing oxygen coverage, Θ_o. Based upon the non-steady-state site balances and the rate equations given in Table 1, the rates of change of oxygen coverage and oxide coverage are determined by the following differential equations:

$$\frac{d\Theta_o}{dt} = 2k_1 C_{O_2} \Theta*^2 - k_7 \Theta_o \exp\left(-\frac{EF}{RT}\right) - k_8 \Theta_o (1 - \Theta_{ox}), \quad (1)$$

$$\frac{d\Theta_{ox}}{dt} = k_8 \Theta_o (1 - \Theta_{ox}) + k_9 C_{OH} \Theta* \exp\left(\frac{EF}{RT}\right) - k_{11} \Theta_{ox} \Theta* \exp\left(-\frac{EF}{RT}\right), \quad (2)$$

where Θ_o is the oxygen surface coverage, Θ_{ox} is the coverage of inactive oxide formation, $\Theta*$ is the free site surface coverage, k_i are the reaction rate parameters defined in Table 2, and C_{O_2} (mol m^{-3}) is the oxygen concentration at the catalyst surface. E (V) is the electrochemical catalyst potential, F (C mol^{-1}) is Faraday's constant, R (J mol^{-1} K^{-1}) is

Table 1
Reaction steps and rate equations for alcohol oxidation mechanism (Gangwal et al. [27])

Reaction step	Rate equation	
$O_2 + 2* \rightarrow 2O*$	$R_1 = k_1 C_{O_2} \Theta*^2$	(I)
$RCH_2OH + *_\rho \rightleftharpoons RCH_2OH*_\rho$	$\Theta_{RCH_2OH} = K_2 C_{RCH_2OH} \Theta*_\rho$	(II)
$RCHO + *_\rho \rightleftharpoons RCHO*_\rho$	$\Theta_{RCHO} = K_{2a} C_{RCHO} \Theta*_\rho$	(IIa)
$RCH_2OH*_\rho + * \rightarrow RCHO*_\rho + 2H^+ + 2e^- + *$	$R_3 = k_3 \Theta_{RCH_2OH} \Theta* \exp(\frac{EF}{RT})$	(III)
$RCH_2OH*_\rho + * + OH^- \rightarrow RCHO*_\rho + H_2O + H^+ + 2e^- + *$	$R_4 = k_4 \Theta_{RCH_2OH} \Theta* C_{OH} \exp(\frac{EF}{RT})$	(IV)
$RCHO*_\rho + * + H_2O \rightarrow RCOOH*_\rho + 2H^+ + 2e^- + *$	$R_5 = k_5 \Theta_{RCHO} \Theta* \exp(\frac{EF}{RT})$	(V)
$RCHO*_\rho + * + OH^- \rightarrow RCOOH*_\rho + H^+ + 2e^- + *$	$R_6 = k_6 \Theta_{RCHO} \Theta* C_{OH} \exp(\frac{EF}{RT})$	(VI)
$O* + H_2O + 2e^- \rightarrow 2OH^- + *$	$R_7 = k_7 \Theta_o \exp(-\frac{EF}{RT})$	(VII)
$O* + *_s \rightarrow O*_s + *$	$R_8 = k_8 \Theta_o (1 - \Theta_{ox})$	(VIII)
$O* + * \rightarrow O*_s + *$	$R_{8a} = k_{8a} \Theta_o \Theta_*$	(VIIIa)
$OH^- + * \rightarrow O*_s + H^+ + 2e^-$	$R_9 = k_9 C_{OH} \Theta* \exp(\frac{EF}{RT})$	(IX)
$RCOOH + *_\rho \rightleftharpoons RCOOH*_\rho$	$\Theta_{RCOOH} = K_{10} C_{RCOOH} \Theta*_\rho$	(X)
$O*_s + H_2O + 2e^- + * \rightarrow 2OH^- + * + *_s$	$R_{11} = k_{11} \Theta_{ox} \Theta* \exp(-\frac{EF}{RT})$	(XI)

Table 2
Kinetic parameters for reaction steps defined in Table 1 (Gangwal et al. [27])

Parameter	Reaction step	Pt/C (dispersion 42%)
k_1 ($m^3\,mol^{-1}\,s^{-1}$)	oxygen adsorption	9.10×10^{-1}
K_2 ($m^3\,mol^{-1}$)	alcohol adsorption	5.78×10^{-2}
K_{2a} ($m^3\,mol^{-1}$)	aldehyde adsorption	5.78×10^{-2}
K_{10} ($m^3\,mol^{-1}$)	acid adsorption	1.29×10^{-1}
k_3 (s^{-1})	alcohol dehydrogenation	5.28×10^{-9}
k_4 ($m^3\,mol^{-1}\,s^{-1}$)	alcohol dehydrogenation (pH)	3.40×10^{-4}
k_5 (s^{-1})	aldehyde dehydrogenation	4.88×10^{-7}
k_6 ($m^3\,mol^{-1}\,s^{-1}$)	aldehyde dehydrogenation (pH)	1.60
k_7 (s^{-1})	oxygen reduction	5.10×10^{6}
k_8 (s^{-1})	oxide formation	1.13×10^{-3}
k_{8a} (s^{-1})	modified oxide formation	$(2.63 \pm 0.09) \times 10^{-3}$
k_9 ($m^3\,mol\,s^{-1}$)	oxide formation (pH)	9.39×10^{-7}
k_{11} (s^{-1})	oxide reduction	$(1.50–2.00) \times 10^{3}$

the ideal gas constant, T (K) is the reaction temperature, and t is time.

The steady-state catalyst potential during alcohol oxidation is based on the mixed potential theory [34,35]. It is assumed that each Pt particle acts as a "short-circuited" electrochemical cell, in which the anodic (alcohol dehydrogenation) and cathodic (oxygen reduction) half-reactions take place at the same rate and the same catalyst potential [25,26]. The catalyst potential is a function of the surface coverages of various reducing and oxidising species [13,36,37]. The catalyst potential is determined by balancing the rate of electrons produced ($R_3 + R_4 + R_5 + R_6 + R_9$) per volume of the catalyst and the rate of electrons consumed ($R_7 + R_{11}$) per volume of the catalyst. The resulting catalyst potential can be expressed by the Nernst equation:

$$E(t) = \frac{RT}{2F} \ln\left(\frac{R_{oxid1} + R_{oxid2}}{R_{red1} + R_{red2} + R_{red3} + R_{red4} + R_{red5}} \right) \quad (3)$$

with

$$R_{oxid1} = k_7 L_t \rho_p \Theta_o, \quad (4)$$

$$R_{oxid2} = k_{11} L_t \rho_p \Theta_{ox} \Theta*, \quad (5)$$

$$R_{red1} = k_3 L_t \rho_p \Theta_{RCH_2OH} \Theta*, \quad (6)$$

$$R_{red2} = k_4 L_t \rho_p C_{OH} \Theta_{RCH_2OH} \Theta*, \quad (7)$$

$$R_{red3} = k_5 L_t \rho_p \Theta_{RCHO} \Theta*, \quad (8)$$

$$R_{red4} = k_6 L_t \rho_p C_{OH} \Theta_{RCHO} \Theta*, \quad (9)$$

$$R_{red5} = k_9 L_t \rho_p C_{OH} \Theta* \quad (10)$$

where k_i are the reaction rate parameters defined in Table 2, L_t is the specific number of platinum surface atoms (i.e., mol Pt_s kg^{-1} catalyst, based on the assumption that one Pt surface atom equals one catalytic site), ρ_p ($kg\,m^{-3}$) is the catalyst particle density, Θ_{RCH_2OH} is the reactant alcohol surface coverage, Θ_{RCHO} is the intermediate aldehyde surface coverage, and C_{OH} ($mol\,m^{-3}$) is the hydroxyl concentration. It should be noted that two important phenomena limit the range of the catalyst potential. First, at a potential lower than 0.4 V RHE, catalyst coverage with adsorbed hydrogen species and CO formation become significant. Second, above a potential of 1.5 V RHE, oxygen gas evolves because of water oxidation. Since these reactions are not taken into account in the kinetic model presented in Table 1, Eq. (3) can only be applied if

$$0.4 \text{ V RHE} < E < 1.5 \text{ V RHE}. \quad (11)$$

2.2. Semi-batch reactor model

In practice, the oxidation reaction is generally carried out with the aqueous alcohol reactant in a batch mode and the oxidant, molecular oxygen, in a continuous mode. For the reaction to take place, oxygen has to be transferred from the gas phase to the liquid phase, through the liquid to the catalyst particle, and finally has to diffuse through the pores to the catalytic site inside the particle. For this work, it was verified that liquid-to-solid mass transport limitation and intraparticle diffusion limitations are not present and hence were not taken into account [38]. The transient material balance

equations for oxygen in the gas phase and in the liquid phase are as follows:

$$\frac{V_G}{RT}\frac{dP}{dt} = F_{V,G}\frac{P^{in}-P}{RT} - k_{GL}a_{GL}V_L(HP - C_L),$$
gas phase (G), (12)

$$V_L\frac{dC_L}{dt} = k_{GL}a_{GL}V_L(HP - C_L) - V_L R_{V,O_2},$$
liquid phase (L), (13)

where V_G (m^3) is the volume of gas in the reactor, P (Pa) is the oxygen partial pressure in the reactor, $F_{V,G}$ ($m^3\,s^{-1}$) is the total volumetric gas flow rate, $k_{GL}a_{GL}$ (s^{-1}) is the volumetric gas-to-liquid mass transport coefficient, H ($mol\,m^{-3}\,Pa^{-1}$) is the Henry coefficient, C_L ($mol\,m^{-3}$) is the oxygen concentration in the liquid phase, V_L (m^{-3}) is the total liquid volume, and R_{V,O_2} ($mol\,m^{-3}\,s^{-1}$) is the overall volumetric oxygen consumption rate:

$$R_{V,O_2} = C_{cat}L_t k_1 \Theta*^2 C_L, \quad (14)$$

where C_{cat} ($kg\,m^{-3}$) is the catalyst concentration. The rate of reaction can also be expressed in terms of the specific consumption of the reactant alcohol, R_{RCH_2OH} ($mol\,kg^{-1}\,s^{-1}$), from Eq. (III) in Table 1 as

$$R_{RCH_2OH} = L_t k_3 \Theta_{RCH_2OH}\Theta* \exp\left(\frac{EF}{RT}\right), \quad (15)$$

where Θ_{RCH_2OH} is the reactant alcohol surface coverage and is calculated from Eq. (II) in Table 1.

The liquid reactant alcohol is in a batch mode and is continuously converting to the product as the reaction progresses; for example, methyl glucoside (MGP) gives methyl glucuronic acid (MG) with methyl aldehydoglucoside (MAGP) as an intermediate. The material balances for the liquid reactant and the products are described as follows:

The rate of disappearance of alcohol to aldehyde is

$$\frac{dC_{RCH_2OH}}{dt} = -C_{cat}R_{RCH_2OH}, \quad (16)$$

$$\frac{dC_{RCHO}}{dt} = C_{cat}(R_{RCH_2OH} - R_{RCHO}), \quad (17)$$

where R_{RCHO} is the rate of aldehyde disappearance and is determined from Eq. (IV) in Table 1 as

$$R_{RCHO} = L_t k_4 \Theta_{RCHO}\Theta* \exp\left(\frac{EF}{RT}\right), \quad (18)$$

where Θ_{RCHO} is the aldehyde surface coverage and is calculated from Eq. (IIa) in Table 1. The rate of acid formation is calculated from the rate of disappearance of the aldehyde as

$$\frac{dC_{RCOOH}}{dt} = C_{cat}R_{RCHO}. \quad (19)$$

The reactor model equations are solved with Matlab software, with the use of the catalyst properties and the experimental conditions as given in Tables 3 and 4. The differential equations, Eqs. (12), (13), (16), (17), and (19), are solved by a stiff ordinary differential equation solver routine (ode23s).

Table 3
Catalyst properties

Catalyst properties	Eggshell Pt/C (Engelhard, code-43545)
Dispersion (%)	42
BET surface area ($m^2\,g^{-1}\,m^{-1}$)	900
Pt content (wt%)	5
Particle size (μm)	35–40
Moisture content (%)	46.88
Porosity (%)	80
Density ($kg\,m^{-3}$)	1050
L_t ($mol\,kg^{-1}$)	0.1078

Table 4
Experimental operating conditions

Operating condition	Semi-batch reactor
pH (–)	8
Degree of conversion (%)	5–30
Temperature, T (K)	323
Catalyst concentration, C_{cat} ($kg\,m^{-3}$)	2
Stirring speed (rpm)	1000
Oxygen partial pressure, P^{in} (kPa)	40
Initial MGP concentration, C_{MGP} ($mol\,m^{-3}$)	100
Initial MG concentration, C_{MG} ($mol\,m^{-3}$)	0
Liquid volume, V_L (m^3)	0.5×10^{-3}
Gas volume, V_G (m^{-3})	0.35×10^{-3}
Volumetric gas flow, $F_{V,G}$ ($m^3\,s^{-1}$)	14×10^{-6}
$k_{GL}a_{GL}$ (s^{-1})	0.4

3. Experimental

3.1. Conditions

In this work, experiments were performed in a stirred three-phase semi-batch reactor. The aqueous alcohol reactant is added in a batch mode. The gaseous oxidant (molecular oxygen) is supplied continuously by a mass flow controller. The oxygen partial pressure is set by the nitrogen flow, also supplied by a mass flow controller. The pH of the reaction medium is kept at a constant level, by controlled addition of a known concentration of an alkali (NaOH). During the reaction, the alcohol reactant is converted to the product acid with time. The acid formation rate is measured through the rate of addition of alkali. The oxygen concentration in the liquid phase is measured with an oxygen electrode. The open circuit electrochemical catalyst potential is measured with a smooth Pt wire as the working electrode and Ag/AgCl, saturated KCl as a reference electrode. A commercial non-uniform (egg shell), 5 wt% Pt on carbon (Engelhard; code-43545) catalyst is used. The properties of the catalyst are listed in Table 3. Experiments were performed under the re-

action conditions listed in Table 4, and further details of the procedure are described elsewhere [38].

3.2. Reaction start-up procedure

Depending on the pretreatment of the catalyst, three different reaction starting procedures are investigated, as follows:

3.2.1. Reductive start-up

For the reductive start-up procedure, the catalyst slurry is prereduced in a hydrogen atmosphere for about 1800 s at 323 K. After it is flushed with nitrogen, the liquid reactant, aqueous alcohol, is added to the slurry, and the experiment is started by a specific partial pressure of oxygen introduced by the gas inlet to the reactor. The details of the experimental procedure are described elsewhere [38].

3.2.2. Oxidative start-up

For the oxidative start-up procedure, the catalyst pretreatment is similar to the reductive start-up. However, before starting the reaction, the catalyst slurry is oxidised by exposure to a 40-kPa partial pressure of gaseous oxygen, for a specific time of 1800 s. The reaction is then started in oxidising medium, by the addition of a known concentration of aqueous alcohol to the reactor.

3.2.3. Inert start-up

The term “inert” means that the reaction is started without any pretreatment of the catalyst. The catalyst slurry is brought to the reaction temperature in a nitrogen atmosphere. The liquid reactant, aqueous alcohol, is added to the aqueous catalyst slurry, at the reaction temperature, and the experiment is started by simultaneous addition of oxygen to the reactor.

4. Results and discussion

4.1. Reductive start-up

Fig. 1a shows the experimentally observed acid formation rate as a function of time for the reductive start-up procedure. The initial acid formation rate obtained is 5.6 mmol $kg^{-1}s^{-1}$. As the reaction progresses the reaction rate clearly drops. This drop is due not only to conversion of the liquid reactant, but also to strong catalyst deactivation. To visualise this catalyst deactivation phenomenon, the observed catalyst potential against time is presented in Fig. 1c. Starting from a reduced catalyst (0.1 V potential) surface, the catalyst potential instantly increases to 0.9 V as soon as the oxygen reaches the catalyst surface; thereafter it slowly increases further and stabilises around 0.97 V. This further increase in the catalyst potential indicates that the catalyst deactivates because of overoxidation [24,25].

In the literature, it has been argued that overoxidation is the result of catalyst deactivation due to carbonaceous deposition and that overoxidation is not the direct cause of catalyst deactivation [4,12]. The simplest way to verify the main cause of the deactivation is to restore the initial rate of reaction by interruption of the oxygen supply to the reactor or to stop the gas-inducing stirrer for a few minutes [30], which facilitates the reduction of the catalyst by the alcohol reactant. Fig. 1a shows that after 2500 s of reaction time, the oxygen supply to the reactor was stopped for about 1100 s and then was started again. There is a temporary sharp increase in the reaction rate, from 1.75 mmol kg^{-1} s^{-1} to 2.23 mmol kg^{-1} s^{-1}, at the initial stage of the regeneration, and then the reaction rate immediately drops. After the oxygen flow is resumed, the rate of reaction is restored to the level of the fresh active catalyst. The catalyst is regenerated by a simple in situ reduction process, which shows that overoxidation is the main cause of deactivation and not the deposition of carbonaceous compounds. However, the magnitude of the recovered reaction rate is not the same as at the beginning of the reaction, because of the drop in the reactant concentration (conversion 17%). The temporary increase in the reaction rate, shortly after the oxygen flow is stopped, may be an indication of the consumption of inactive oxide together with the negative order dependence on oxygen concentration, which has been demonstrated in our previous modelling work [39]. The reduction of the catalyst can also be seen through the drop in the measured electrochemical catalyst potential (Fig. 1c), which reaches 0.4 V. As soon as the oxygen flow is resumed, the catalyst potential follows its previous track; however, it reaches a higher level of 0.97 V more quickly.

Fig. 1a shows that the dynamic semi-batch reactor model, which assumes overoxidation to be the main cause of catalyst deactivation, is well able to describe the observed reaction rates. The high initial catalytic activity followed by the strong catalyst deactivation accompanied by reactant conversion is accurately described by the model. In order to mimic the experimental data, after a simulation time of 2500 s, the gas-phase oxygen partial pressure in the model was forced to zero for 1100 s and then switched back to its original value. The reactor model with the electrochemical kinetics clearly demonstrates that the catalyst activity is fully regenerated, and overoxidation is the main cause of the deactivation. In order to describe a temporary increase in the acid formation rate as observed in the experiment at the beginning of the reactivation period, diffusion limitation inside the catalyst particle has to be considered in the model [39]. Immediately after the oxygen partial pressure is set to zero, the model shows a temporary increase in the reaction rate (Fig. 1b). However, the magnitude of this increased rate is lower than that observed in the experiment. This may be due to the fact that the model insufficiently accounts for the oxygen storage capacity of the catalyst support and the platinum oxide.

The calculated potentials presented in Fig. 1c, show the right magnitude for the increase in the reaction rate with

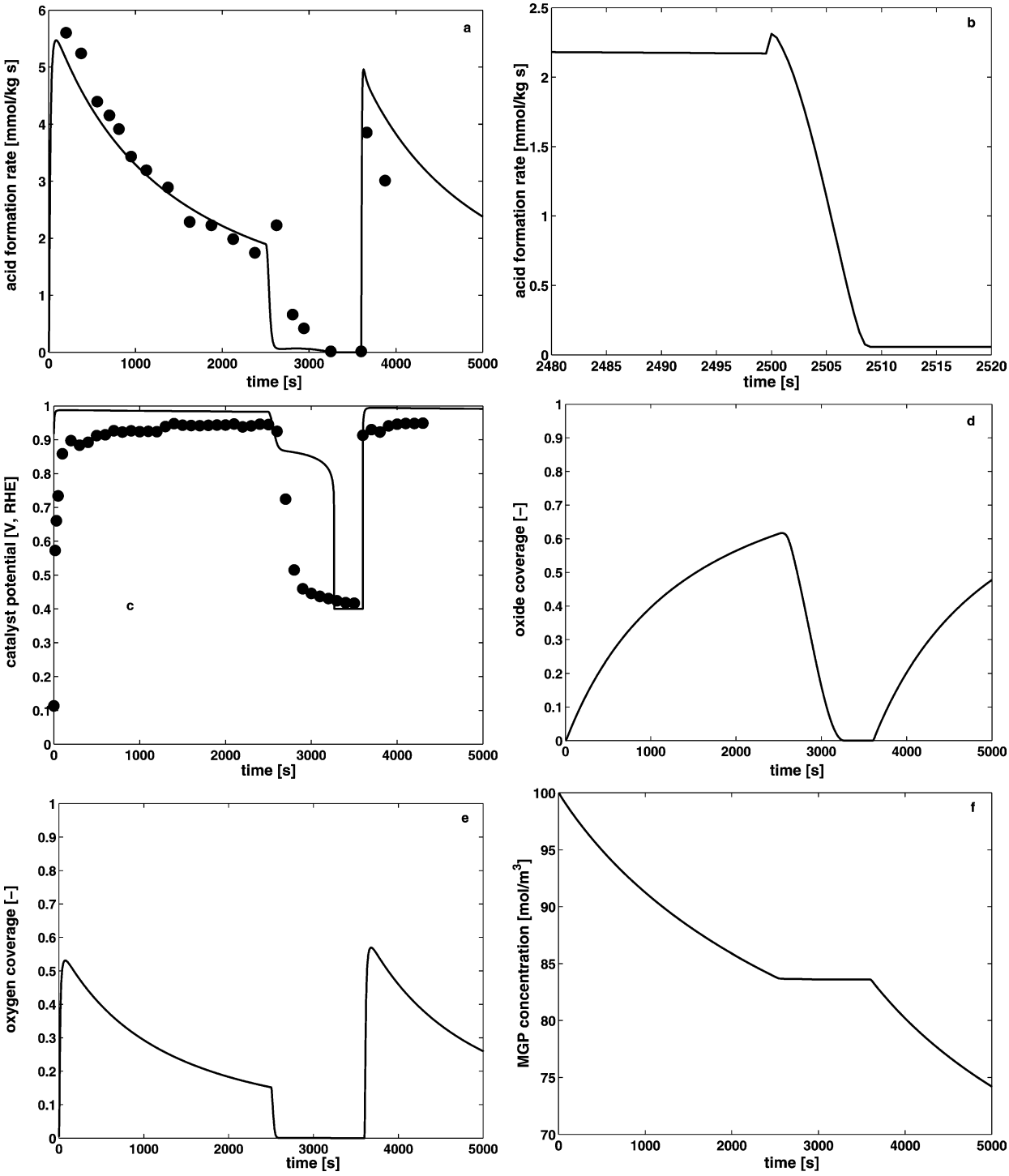

Fig. 1. Effect of the reductive startup procedure: (a) acid formation rate; (b) enlarged view of the acid formation rate using diffusion model, for simulating the reactivation period; (c) electrochemical catalyst potential; (d) oxide coverage; (e) oxygen coverage; and (f) MGP concentration. The oxygen supply stopped from 2500 to 3600 s. Symbols represent experimental data and lines represent model results.

increase in potential from the reduced state followed by catalyst deactivation with time, corresponding to an oxidised potential level of approximately 1 V. During the reduction period, the drop in the model predicted potential is smaller, compared with the measured catalyst potential. However, after some time, the model shows a rapid drop in the potential to a level of 0.4 V. There is a discrepancy between the model and the experiments because the measured electrochemical catalyst potential is quite dynamic, as it is a mixed potential of colliding catalyst particles, the reaction mixture, and the smooth Pt wire, whereas in the model the removal of oxide is a relatively slow process. As soon as the oxygen pressure

is switched back to its original value, the potential increases faster and stabilizes to a slightly higher level (1 V) than the original level (0.99 V), similar to the experimentally measured catalyst potential.

The degree of catalyst deactivation due to overoxidation is presented as the simulated oxide coverage against time in Fig. 1d. After 2500 s, approximately 60% ($\Theta_{ox} = 0.58$) of the catalyst surface is covered with inactive platinum oxide. During the reduction time, the drop in oxide coverage coincides with the catalyst potential. It can be seen from the figure that at 3200 s the oxide coverage decreases to zero, which means 700 s of reduction time is sufficient for regeneration of the catalyst. This means that with this model the reduction period can be optimised, which is essential to avoid carbonaceous deposits due to prolonged exposure of the reduced catalyst to organic compounds [16,17].

Fig. 1e shows the simulated oxygen coverage with time. The initial oxygen coverage (approx. 0.5) decreases with time because of the increase in oxide formation. During the reduction period the coverage quickly drops to zero. As soon as the oxygen pressure is switched to its original value, the oxygen coverage at the catalyst surface increases, goes to a higher level because of lower alcohol coverage (conversion), and drops again because of overoxidation. Fig. 1f shows the simulated concentration of the reactant alcohol, MGP, as a function of time. It can be seen that the calculated conversion, from MGP concentration data, is around 26% over 5000 s of the simulation time. Within this conversion level, it can be accepted that the MGP oxidation has close to 100% selectivity [24].

4.2. Oxidative start-up

Fig. 2a shows the experimentally observed acid formation rate as a function of time for the oxidative start-up procedure. The catalyst slurry, after reduction with hydrogen, is oxidised with a 40 kPa partial pressure of oxygen, for about 1800 s, in the absence of the alcohol reactant. The reaction is started by the addition of a known amount of alcohol reactant to the catalyst slurry, in the presence of oxygen. The initial acid formation rate obtained is 4.21 mmol kg^{-1} s^{-1}, which is 1.3 times lower than the initial rate for the reductive start-up. As the reaction progresses the drop in the reaction rate can clearly be seen. This drop occurs not only because of conversion of the reactant but also because of strong catalyst deactivation. Again to visualise the catalyst deactivation, the observed catalyst potential against time is presented in Fig. 2b. In the oxidising medium the catalyst has a potential of about 1.1 V, and as soon as the alcohol reactant is added to the catalyst slurry the potential drops to 0.9 V, and thereafter it slowly increases to 0.97 V and stabilises. This increase in the catalyst potential indicates that the catalyst has deactivated.

To verify the mechanism of deactivation, the regeneration procedure as described in the previous section is followed. Fig. 2a shows that after 4000 s of run time, the oxygen supply to the reactor was stopped for about 800 s and started again. There is a temporary increase in the reaction rate, from 1.95 to 3.45 mmol kg^{-1} s^{-1}, at the initial stage of the regeneration and then the reaction rate immediately drops. This temporary increase in the reaction rate is almost 3 times higher than that for the reductive start-up. After the oxygen flow is resumed, the rate of reaction is restored to the level of fresh active catalyst. The catalyst is regenerated by the simple in situ reduction process, which confirms that overoxidation is the main cause of deactivation. The reduction of the catalyst can also be seen through the drop in the measured catalyst potential (Fig. 2b), which reaches 0.4 V. As soon as the oxygen flow is resumed, the catalyst potential follows its previous track; however it rather quickly reaches a higher level of 0.97 V.

For modelling of the oxidative start-up, the semi-batch reactor model has been modified, containing two parts: first the oxidised period (no reaction), where the reactant alcohol is not present, followed by the reaction period, with the standard set of equations.

For the oxidised period (no reaction), Eqs. (1), (2), (12), and (13) are used, whereas the catalyst potential Eq. (3) is modified, because of the absence of alcohol reactant and reaction products, as follows:

$$E = \frac{RT}{2F}\ln\left(\frac{R_{oxid1} + R_{oxid2}}{R_{red5}}\right). \tag{20}$$

It is found that during the preoxidising period, in the absence of the alcohol reactant, the model predicts a high degree of catalyst deactivation ($\Theta_{ox} = 0.8$), which results in a much lower reaction rate (not shown here) compared with the observed reaction rate. However, after the reduction period, the model shows complete regeneration of the catalytic activity and gives an accurate description of the reaction rates thereafter, which duplicates the reductive start-up. In order to describe the initial observed reaction rates, for the oxidative start-up, the kinetic step (VIII), in Table 1, is modified to step (VIIIa). It is assumed that free sites are needed for the transformation of chemisorbed oxygen into inactive oxide. It can be envisaged that chemisorbed oxygen, in the absence of co-reactants, forms a regular layer on the platinum surface, which only decomposes into inactive oxide, depending on the degree of layer disruption (creation of free sites). This is similar to the "oxygen passivation" phenomena in corrosion science, or place exchange mechanisms observed in electrochemistry [40]. This is also in agreement with Dirkx and van der Baan [28], who have found that catalyst deactivation due to overoxidation is higher in the presence of the reactant alcohol (reaction) than in the absence of the reactant. The kinetic parameter, k_{8a}, of the modified step, (VIIIa) in Table 1, is estimated with the use of former experimental data, obtained under different pH conditions [27], with the other parameters kept fixed. It is verified that the results presented for the reductive start-up are not altered, because of the modification in this step. The parameter k_{8a} is exchanged for $k_{8a} \times \bar{\Theta}*$ in the model, and the average free site cover-

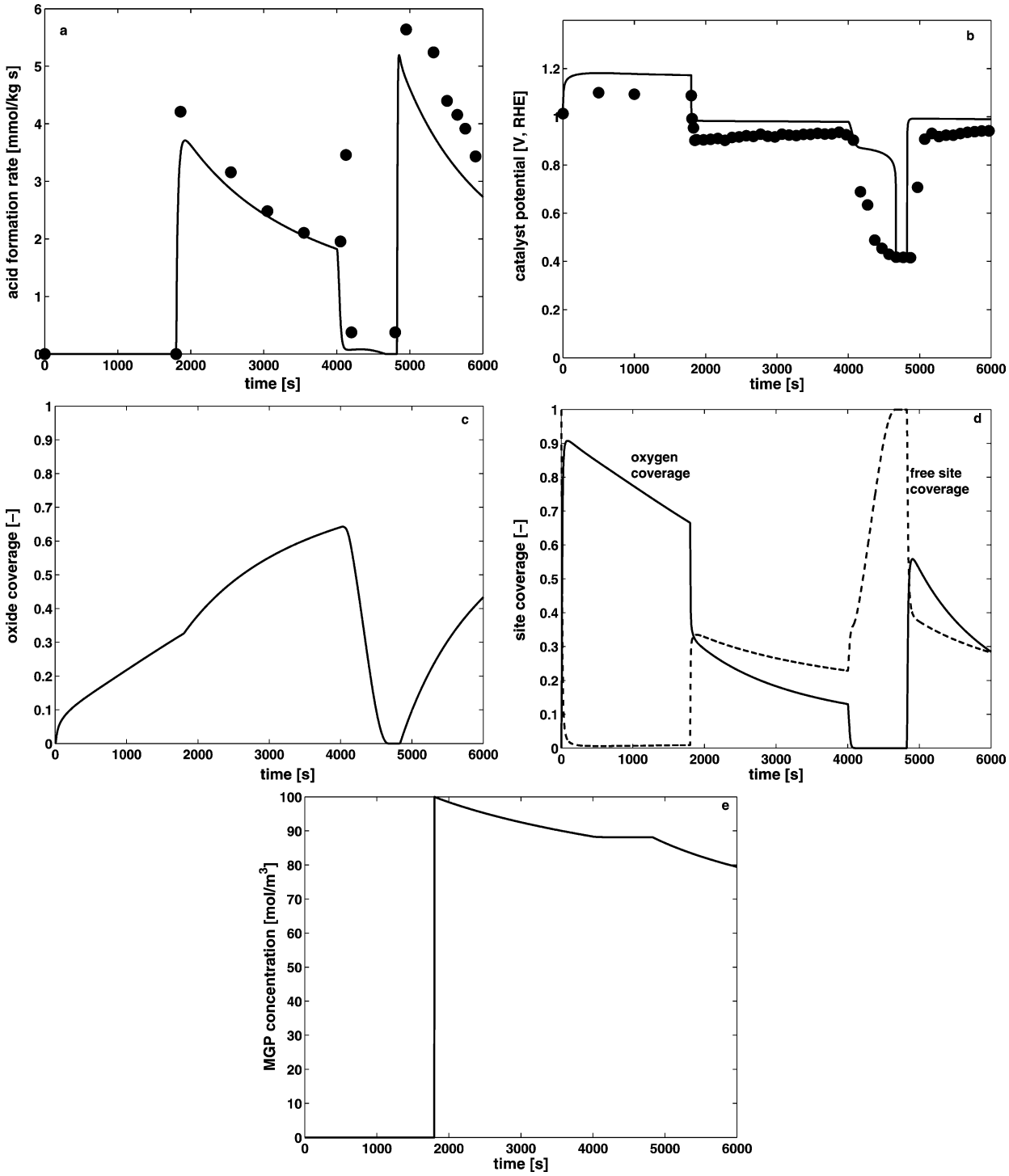

Fig. 2. Effect of the oxidative startup procedure: (a) acid formation rate; (b) electrochemical catalyst potential; (c) oxide coverage; (d) oxygen (continuous line) and free site coverage (dashed line); and (e) MGP concentration. The reactant alcohol, MGP, is added after 1800 s and the oxygen supply stopped from 4000 to 4800 s. Symbols represent experimental data and lines represent model results.

age, $\bar{\Theta}*$, during the reaction is approximately 0.43, which results in $k_{8a} \sim 2.35 \times k_8$.

Fig. 2a shows that the reactor model is well able to describe the observed reaction rates. The acid formation rate after the pre-oxidation period (no reaction) is now properly simulated. In order to mimic the experimental data, after a simulation time of 4000 s, the gas-phase oxygen partial pressure in the model was forced to zero for 800 s and then switched back to its original value. The model clearly demonstrates that the catalyst activity is fully regenerated and overoxidation is the main cause of catalyst deactivation. Immediately after the oxygen partial pressure is set to zero,

the model shows a temporary increase in the reaction rate. However, the magnitude of the increased rate is lower than observed in the experiment, similar to the reductive start-up simulations.

The calculated potentials presented in Fig. 2b show that the model adequately describes the measured electrochemical catalyst potentials. In the oxidised period the electrochemical catalyst potential reaches a high value, around 1.2 V, compared with the reaction period. The potential decreases to a lower value of 0.99 V with the addition of the alcohol reactant. However, during the reduction period, the model predicts a slower drop in the catalyst potential compared with the measured potential, similar to that for the reductive start-up.

The degree of catalyst deactivation due to overoxidation is presented as the simulated oxide coverage against time in Fig. 2c. During the pre-oxidation period of 1800 s, approximately 22% ($\Theta_{ox} = 0.22$) of the catalyst surface is covered with inactive platinum oxide. It can be determined that after approximately 33 h of continuous exposure of the catalyst to the oxygen supply, full coverage with inactive platinum oxide ($\Theta_{ox} = 1$) is obtained. After the addition of the reactant alcohol, the reaction starts but the level of the oxide coverage remains the same. This shows that the reactant alcohol is unable to reduce the oxide in the presence of oxygen, which confirms that the reactant MGP is a weak reducing compound. However, the oxygen coverage presented in Fig. 2d drops from 0.8 to below 0.4, which has a slight effect on the catalyst potential, lowering its value from 1.2 to 1 V (Fig. 2b).

After 4000 s of simulation time the model shows 60% catalyst deactivation, whereas the same degree of catalyst deactivation (60%) was obtained after 2500 s with the reductive start-up. This means that a higher catalyst deactivation rate is observed with reaction than without reaction. In practice, catalyst deactivation seems to be proportional to the turnover frequency [28]. This can be understood by considering that the alcohol dehydrogenation rate, step (III) in Table 1, and the inactive oxide formation rate, steps (VIIIa) and (IX), are proportional to the number of available free sites. During the reduction time, the drop in oxide coverage coincides with the catalyst potential. The oxide is completely removed after 800 s of catalyst reduction, which indicates complete regeneration of the catalyst.

Fig. 2d shows the simulated oxygen coverage and free site coverage with time. The oxidative start-up leads to a higher initial oxygen coverage (approx. 0.9) than the reductive start-up (approx. 0.5). As soon as the reactant alcohol is added to the slurry, the oxygen coverage drops from a level of 0.8 to below 0.4, whereas the free site coverage increases to 0.38. The oxygen coverage further decreases with time due to an increase in oxide formation. The increased number of available free sites contributes to overoxidation during the reaction, through kinetic steps (VIIIa) and (IX) in Table 1. During the reduction period the oxygen coverage quickly drops to zero, and the free site coverage reaches 1. When the oxygen pressure is switched to its original value, the oxygen coverage at the catalyst surface increases and goes to a higher level (approx. 0.6), because of a lower alcohol coverage (conversion), and drops again because of overoxidation. Fig. 2e shows the simulated concentration of the reactant alcohol, MGP, as a function of time. It can be seen that the calculated conversion, from MGP concentration data, is around 22% over 6000 s of the simulation time.

4.3. Inert start-up

Fig. 3a shows the experimentally observed acid formation rate as a function of time for the inert start-up procedure; that is, the catalyst was used from the shelf. It can be seen that the catalyst shows hardly any activity. The inert start-up represents an extreme case of the oxidative start-up. The initial rate obtained was only 0.3 mmol kg^{-1} s^{-1}, which is nearly 19 times lower than the reductive start-up and 14 times lower than the oxidative start-up. Furthermore, to understand the cause of such a low activity, the oxygen flow was stopped after 3500 s for about 1000 s and started again. It can be seen from the figure that the catalyst was fully regenerated and an acid formation rate of 5.8 mmol kg^{-1} s^{-1} was obtained, which is of the same magnitude as for the reductive start-up. This shows that with the inert start-up procedure, before the reaction was started, the catalyst was fully overoxidised. The initial reaction rate is close to the reaction rate obtained by Dirkx and van der Baan [29] for an overoxidised catalyst. The complete reactivation of the catalyst confirms that overoxidation is the main cause of the catalyst deactivation. The temporary increase in the reaction rate, from 0.5 to 1.1 mmol kg^{-1} s^{-1}, at the initial stage of the regeneration, matches the findings from the other start-up procedures.

To understand catalyst deactivation, the observed electrochemical catalyst potential against time is presented in Fig. 3b. Starting from an oxidised surface with a potential around 1 V, after addition of the reactant, the potential drops to a lower value of 0.9 V. The catalyst potential stays at the same level over the reaction time. This inertness of the catalyst potential corresponds to the unaltered concentration (no conversion) of the reactant alcohol. During the reduction period, the catalyst potential drops to 0.4 V. As soon as the oxygen flow is resumed, the catalyst potential instantaneously increases to 0.9 V and quickly reaches 0.97 V during the reaction, where it stabilises, confirming the overoxidation.

For modelling of the inert start-up, it is assumed that the catalyst is fully oxidised, that is, there is a high coverage of oxide ($\Theta_{ox} \approx 0.9$). In agreement with the previous section, the modified kinetic step (VIIIa) is used to determine the inactive oxide formation. Fig. 3a shows that the reactor model is well able to describe the observed low reaction rates. In order to mimic the experimental data, after a simulation time of 3500 s, the gas-phase oxygen partial pressure in the model was forced to zero for 1000 s and then switched back to its

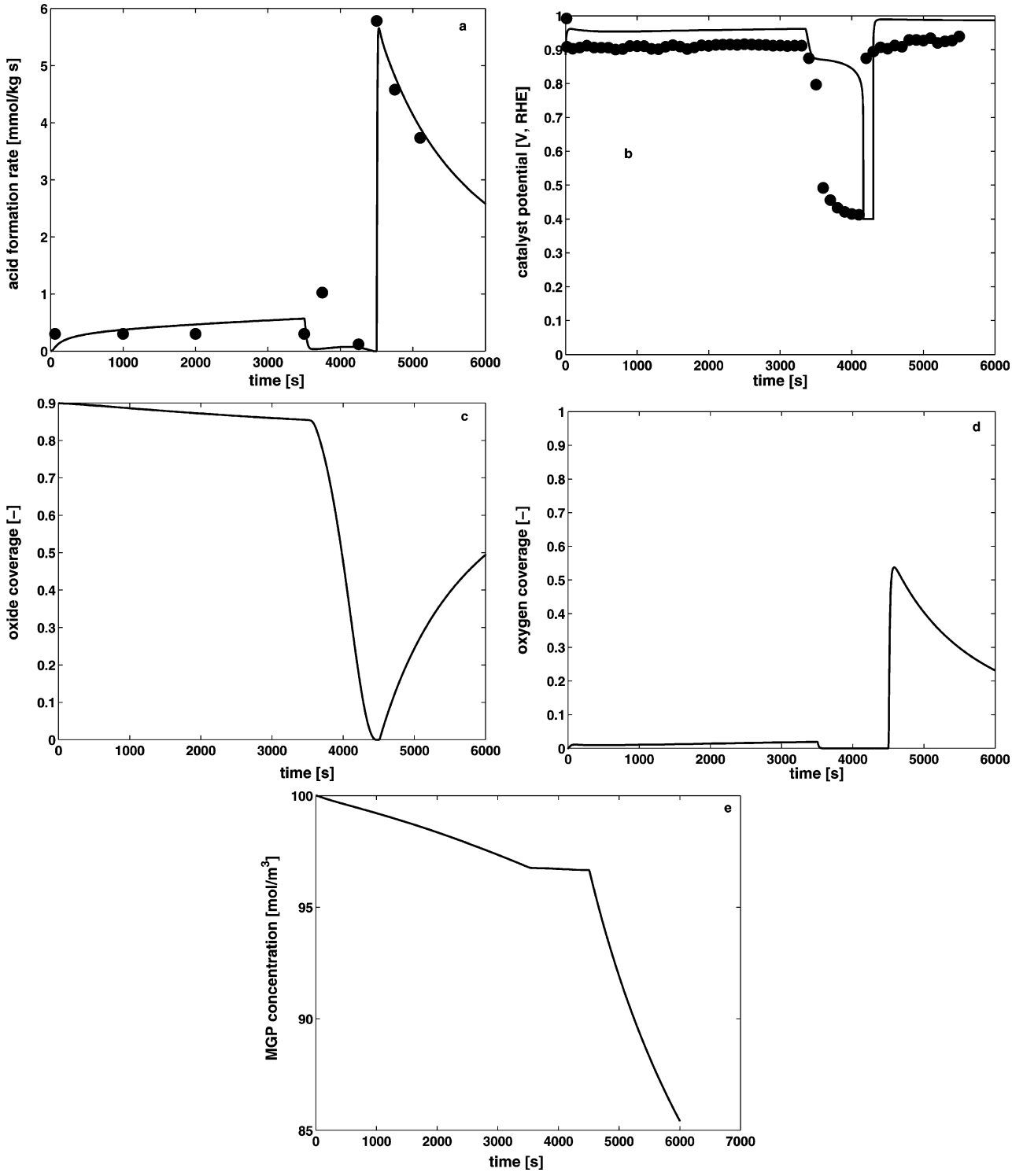

Fig. 3. Effect of the inert startup procedure: (a) acid formation rate; (b) electrochemical catalyst potential; (c) oxide coverage; (d) oxygen coverage; and (e) MGP concentration. The oxygen supply stopped from 3500 to 4600 s. Symbols represent experimental data and lines represent model results.

original value. The model clearly demonstrates that the catalyst activity is fully regenerated and overoxidation is the main cause of the deactivation. Immediately after the oxygen partial pressure was set to zero, the model showed a temporary increase in the reaction rate. However, the magnitude of the increased rate was lower than observed in the experiment, similar to that for the reductive start-up.

The calculated potentials presented in Fig. 3b properly describe the observed electrochemical catalyst potential. During the reduction period the drop in the model predicted

potential is smaller compared with the measured catalyst potential, as observed for the other start-ups. The potential then drops to the level of 0.4 V, and, as soon as the oxygen pressure is switched back to its original value, the potential increases faster and stabilizes at a higher level (1 V) than the original level (0.95 V), similar to the experimentally measured catalyst potential.

Fig. 3c shows the simulated oxide coverage against time. The oxide coverage remains at a high level, for a long period, as assumed at the beginning of the reaction ($\Theta_{ox} = 0.9$). During the reduction period, the oxide coverage drops to zero after 1000 s. The model clearly demonstrates that the catalyst activity is fully regenerated.

Fig. 3d shows the simulated oxygen coverage with time. It can be seen that the oxygen has insignificant coverage on the catalyst surface, which is due to a high oxide coverage. This also indicates a low activity of the catalyst. During the reduction period, the coverage becomes zero. As soon as the oxygen pressure is switched to its original value, the oxygen coverage at the catalyst surface increases and goes to a higher level of 0.5, similar to that for the reductive start-up. It can also be seen that the oxygen coverage further decreases because of overoxidation. Fig. 3e shows the simulated concentration of the reactant alcohol, MGP, as a function of time. It can be seen that the calculated conversion, from MGP concentration data, is around 15% over 6000 s of simulation time.

5. Conclusions

In this work the effect of the reaction start-up procedure on the oxidation of methyl α-D-glucopyranoside was investigated. Results have been obtained with experiments performed in a stirred slurry semi-batch reactor with Pt on carbon catalyst and molecular oxygen as oxidant. The reductive start-up case gives a nearly 1.3 times higher initial reaction rate than the oxidative start-up case and a nearly 19 times higher initial rate than the inert start-up case. It has been demonstrated, with the help of experiments and the recently developed electrochemical reaction model, that independently of the start-up procedure, overoxidation is the main cause of catalyst deactivation. These results can be generalised for the oxidation of weakly reducing compounds, under oxygen-rich conditions in a weakly alkaline medium. As the reaction progresses, the conversion of the reactant alcohol increases, the rate of oxygen supply becomes higher than the rate of reaction, and the catalyst deactivates because of overoxidation. The results obtained in experiments are validated with the model. The experimental regeneration period can be optimised with the model, to avoid carbonaceous deposits on the reduced catalyst. The observed catalyst potential gives useful information on the oxidation state of the catalyst. The electrochemical model can describe well the observed catalyst potential at different start-up conditions. A modified kinetic step, which considers that free sites are needed for transformation of chemisorbed oxygen into inactive oxide, gave a good description of the oxidative start-up. Investigation of the effect of varying oxygen partial pressure, length of the pre-oxidising period, pH, and metal crystallite size on the initial reaction rate would give useful additional data to verify or adjust the kinetic equations that describe overoxidation.

References

[1] T. Mallat, A. Baiker, Chem. Rev. 104 (2004) 3037.
[2] A.F. Lee, J.J. Gee, H.J. Theyers, Green Chem. 2 (2000) 279.
[3] H. van Bekkum, in: F.W. Lichtenthaler (Ed.), Carbohydrate as Organic Raw Materials, Wiley–VCH, Weinheim, 1990, p. 289.
[4] T. Mallat, A. Baiker, Catal. Today 19 (1994) 247.
[5] M. Besson, P. Gallezot, Catal. Today 57 (2000) 127.
[6] K. Heyns, H. Paulsen, Adv. Carbohydr. Chem. 17 (1962) 169.
[7] H.G.J. de Wilt, H.S. van der Baan, Ind. Eng. Chem. Prod. Res. Develop. 11 (1972) 374.
[8] G. de Wit, J.J. de Vlieger, A.C. Kock-van Dalen, R.H. Rob Laroy, A.J. van Hengstum, A.P.G. Kieboom, H. van Bekkum, Carbohydr. Res. 91 (1981) 125.
[9] R. DiCosimo, G.M. Whitesidesm, J. Phys. Chem. 93 (1989) 768.
[10] J.H.J. Kluytmans, A.P. Markusse, B.F.M. Kuster, G.B. Marin, J.C. Schouten, Catal. Today 57 (2000) 143–155.
[11] T. Mallat, A. Baiker, L. Botz, Appl. Catal. A 86 (1992) 147.
[12] T. Mallat, Z. Bodnar, P. Hug, A. Baiker, J. Catal. 153 (1995) 131.
[13] J.F.E. Gootzen, A.H. Wonders, A.P. Cox, W. Visscher, J.A.R. van Veen, J. Mol. Catal. A 127 (1997) 113.
[14] C. Keresszegi, T. Borgi, T. Mallat, A. Baiker, J. Catal. 211 (2002) 244.
[15] A.F. Lee, K. Wilson, Green Chem. 6 (2004) 37.
[16] T. Mallat, Z. Bodnar, A. Baiker, O. Greis, H. Strubig, A. Reller, J. Catal. 142 (1993) 237.
[17] C. Bronnimann, Z. Bodnar, P. Hug, T. Mallat, A. Baiker, J. Catal. 150 (1994) 199.
[18] J.H. Vleeming, B.F.M. Kuster, G.B. Marin, F. Oudet, P. Courtine, J. Catal. 166 (1997) 148.
[19] H.E. van Dam, A.P.G. Kieboom, H. van Bekkum, Appl. Catal. 33 (1987) 361.
[20] P.J.M. Dijkgraaf, H.A.M. Duisters, B.F.M. Kuster, K. van der Wiele, J. Catal. 112 (1988) 337.
[21] Y. Schuurman, B.F.M. Kuster, K. van der Wiele, G.B. Marin, Appl. Catal. A 25 (1992) 31.
[22] J.H. Vleeming, F.A. de Bruijn, B.F.M. Kuster, G.B. Marin, Stud. Surf. Sci. Catal. 88 (1994) 467.
[23] F.A. de Bruijn, B.F.M. Kuster, G.B. Marin, Appl. Catal. A 145 (1996) 351.
[24] J.H. Vleeming, B.F.M. Kuster, G.B. Marin, Ind. Eng. Chem. Res. 36 (1997) 3541.
[25] T. Mallat, A. Baiker, Top. Catal. 8 (1999) 115.
[26] T. Mallat, A. Baiker, Catal. Today 24 (1995) 143.
[27] V.R. Gangwal, J. van der Schaaf, B.F.M. Kuster, J.C. Schouten, J. Catal. 229 (2005) 389.
[28] J.M.H. Dirkx, H.S. van der Baan, J. Catal. 67 (1981) 1.
[29] J.M.H. Dirkx, H.S. van der Baan, J. Catal. 67 (1981) 14.
[30] P.J.M. Dijkgraaf, M.J.M. Rijk, J. Meuldijk, K. van der Wiele, J. Catal. 112 (1988) 329.
[31] L. Jelemensky, B.F.M. Kuster, G.B. Marin, Catal. Let. 30 (1995) 269.
[32] L. Jelemensky, B.F.M. Kuster, G.B. Marin, Chem. Eng. Sci. 51 (10) (1996) 1767.
[33] L. Jelemensky, B.F.M. Kuster, G.B. Marin, Ind. Eng. Chem. Res. 36 (1997) 3065–3074.

[34] C. Wagner, W. Traud, Z. Electrochem. 44 (1938) 391.
[35] M. Spiro, Chem. Soc. Rev. 15 (1986) 141.
[36] G. Horanyi, Catal. Today 19 (1994) 285.
[37] A.P. Markusse, B.F.M. Kuster, J.C. Schouten, Catal. Today 66 (2001) 191.
[38] V.R. Gangwal, J. van der Schaaf, B.F.M. Kuster, J.C. Schouten, Catal. Today 96 (2004) 223.
[39] V.R. Gangwal, B.G.M. van Wachem, B.F.M. Kuster, J.C. Schouten, Chem. Eng. Sci. 57 (2002) 5051.
[40] B.E. Conway, Prog. Surf. Sci. 49 (1995) 331.